Hydroxyl Radical Footprinting of DNA Complexes of the Ets Domain of PU.1 and Its Comparison to the Crystal Structure†

Petra Gross,‡ Cheryl H. Arrowsmith,§ and Robert B. Macgregor, Jr.*,‡

Department of Pharmaceutical Sciences, University of Toronto, Toronto, Ontario M5S 2S2, Canada, and Department of Medical Biophysics, University of Toronto and Ontario Cancer Institute, Toronto, Ontario M5G 2M9, Canada

Received October 20, 1997; Revised Manuscript Received January 20, 1998

ABSTRACT: Hydroxyl radical footprinting has been used to probe interactions in complexes between the ets domain of the murine transcription factor PU.1 and three different DNA restriction fragments, each containing one copy of the recognition sequence 5′-GGAA-3′. Two natural PU.1 binding sites, the SV40 enhancer site and the λB motif of Ig λ2−4 enhancer, were used as well as the PU.1 binding site present in the crystallized PU.1−DNA complex [Kodandapani, R., Pio, F., Ni, C.-Z., Piccialli, G., Klemsz, M., McKercher, S. R., Maki, R. A., and Ely, K. R. (1996) *Nature 380*, 456−460]. The footprints obtained for the three different DNA sequences are almost identical. The extent of contact with the protein was monitored for every base in the complex. Two concentration-dependent cleavage sites on the complementary TTCC strand are evidence of a specific interaction between PU.1 and the DNA. Two more protection sites and a hypersensitive cleavage site on the GGAA strand were observed. Although these data confirm the global structure of the PU.1−DNA complex as suggested by crystallography, the footprinting data reveal differences between the protein−DNA contacts in solution and in the crystal state. An additional interaction site not present in the crystal structure was observed by hydroxyl radical footprinting.

The PU.1 transcription factor is a member of the ets gene family. It plays an important role in normal development by regulating the differentiation of mast cells and macrophages and in the maturation of B cells (*1*). The ets proteins share a conserved 85 amino acid DNA binding domain, the so-called ets domain, that recognizes the sequence 5′-GGAA-3′ flanked by more variable but not random 5′ and 3′ sequences. These proteins bind the DNA as monomers. PU.1 is the least conserved member of the ets family and shares a 35% homology with ETS-1, the first ets protein that was characterized (*1, 2*).

The secondary structure of the ets domain was solved by NMR for ETS-1 (*3*) and Fli-1 (*4*). Therein, the ets domain is characterized as a "winged helix−turn−helix" DNA binding motif. Recently, the three-dimensional structures of ets protein−DNA complexes have appeared in the literature (*4*−*7*). The crystal structure of PU.1 bound to DNA presents a new pattern for a helix−turn−helix DNA binding motif that is better described as a loop−helix−loop architecture (*5*). In the crystal the DNA is bent toward the protein by 8° and curved almost uniformly along the 16-bp[1] fragment. The protein domain consists of three α-helices and a four-stranded antiparallel β-sheet. Three regions of the protein make contact with the DNA: the recognition helix (α3), the loop between β-strands 3 and 4 (a "wing"), and the loop between helices 2 and 3, which is actually the turn in the helix−turn−helix motif. Four highly conserved amino acids are involved in these contact sites. Two conserved arginines from the recognition helix interact directly with the major groove of the core GGAA sequence. A lysine from the wing binds the DNA phosphate backbone upstream from this sequence and another lysine from the loop between α2 and α3 forms a salt bridge with the backbone downstream and on the opposite strand. It was also reported that mutation of any of these amino acids abolished DNA binding. Furthermore, a network of well-ordered solvent molecules was observed in the major groove of the DNA.

The structure of the ets domain of another ets protein, Fli-1, has been studied in the presence of a 16-bp oligonucleotide by NMR spectroscopy (*4*). The comparison of the ets domains of PU.1 and Fli-1 demonstrated the importance of interactions mediated by amino acids conserved between the ets family in DNA recognition (*6*). The structure of the ets domain of ETS-1 bound to a 17-bp DNA fragment was solved by NMR (*7*). This study also suggests a bending of the DNA toward the protein and an ets domain containing a helix−turn−helix DNA binding motif.

† This work was supported in part by a research scholarship from the Deutsche Forschungsgemeinschaft to P.G., and grants from the National Science and Engineering Research Council of Canada (to R.B.M.) and the Medical Research Council of Canada (to C.H.A.). C.H.A. is an MRC Scholar.

* Address correspondence to this author at Department of Pharmaceutical Sciences, University of Toronto, 19 Russell St., Toronto, Ontario M5S 2S2, Canada. Phone (416) 978-7332; Fax (416) 978-8511; E-mail macgreg@phm.utoronto.ca.

‡ Department of Pharmaceutical Sciences.

§ Department of Medical Biophysics.

[1] Abbreviations: bp, base pair; dsDNA, double-stranded DNA; BSA, bovine serum albumin; dNTP, deoxyribonucleotide triphosphate; DTT, dithiothreitol; PMSF, phenylmethanesulfonyl fluoride; DBD, DNA binding domain.

S0006-2960(97)02591-9 CCC: $15.00
Published on Web 03/21/1998

Hydroxyl radical footprinting has been shown to resolve the interactions in protein−DNA complexes on a single base level. Hydroxyl radicals react with the backbone of the DNA with almost no sequence specificity, yielding a very uniform cutting pattern. Bands with reduced intensities in the footprinting gel pattern reveal bases that are protected from radical-induced cleavage by protein contacts or conformational changes in the DNA structure. Since a hydroxyl radical is roughly the size of a water molecule, the footprints accurately reflect the accessibility of solvent to the DNA in a given complex (*8*).

Detailed information about the structure and the energetics of protein−DNA interactions have been obtained from hydroxyl radical footprints. The λ bacteriophage repressor and Cro proteins were shown to bind only to one side of the DNA helix at their target sequence (*8*). Analysis of gel patterns produced by hydroxyl radical cleavage were used to determine DNA contacts of the archetypal zinc finger protein TFIIIA (*9*). A binding model of the transcription factor TFIIB to the TATA binding protein complex with DNA was proposed using hydroxyl radical footprinting and the gel pattern was mapped to a crystal structure model (*10*). The hydroxyl radical protection assay for an ETS-1−DNA complex exhibited protection sites on both strands (*2*).

In this paper, we present high-resolution hydroxyl radical footprinting data on complexes between the ets domain of murine PU.1 and DNA restriction fragments containing a single ets consensus sequence. The sequence of the ets domain of murine PU.1 is identical to that of the human PU.1 ets domain (*1*). Three different target DNA sequences were analyzed in the footprinting experiments: the DNA sequence used in the crystal structure, allowing direct comparison to the crystal structure (*5*); a 17-bp region of the SV40 enhancer (*11*); and a 23-bp region within the λB site of an Ig λ2−4 enhancer (*11, 12*). The DNA bases on both strands that are in close contact with the protein are monitored. Three contact sites, in agreement with the crystal structure, and an additional binding site were found (*5*).

MATERIALS AND METHODS

Enzymes and Chemicals. All restriction enzymes, BSA, and T4 polynucleotide kinase were purchased from New England Biolabs Inc.; T4 DNA ligase was from Boehringer Mannheim; *Taq* DNA polymerase came from Gibco BRL. DNase I, the dNTPs, and poly(dI-dC)·poly(dI-dC) were obtained from Pharmacia Biotech. Thrombin came from Calbiochem-Novabiochem Corp. Ammonium iron(II) sulfate hexahydrate and L-ascorbic acid (sodium salt) were from Aldrich; EDTA (disodium salt) and hydrogen peroxide (as a 30% aqueous solution) came from Fisher Biotech. Radioactive [γ-^{32}P]ATP was purchased from Amersham Corp.

DNA Preparation. Single-stranded 61-base oligonucleotides containing the following central sequences were synthesized (Biotech Service Centre, University of Toronto): A, 5′-AAAAAGGGGAAGTGGG-3′; B, 5′-TCCCACTTCCCCTTTT-3′; C, 5′-CTGAAAGAGGAACTTGG-3′; D, 5′-CCAAGTTCCTCTTTCAG-3′; E, 5′-AAATAAAAGGAAGTGAAA-3′; F, 5′-TTTCACTTCCTTTTATT-3′. Each oligonucleotide was phosphorylated using T4 polynucleotide kinase and A was annealed with B, C with D, and E with F. The resulting dsDNA inserts were ligated into the *Hin*dIII binding site of pBluescript II SK$^-$ plasmid (Stratagene, Inc.) yielding three new plasmids: pCRYSK, pPUSK, and pLBSK. The orientation of the inserts in these plasmids was determined by chemical sequencing using the base specific reactions for G and G + A (*13*). The end-labeled DNA fragments used in the footprinting experiments were prepared as follows. Two PCR primers, P1, 5′-CGAGGTCGACGGTATCGATA-3′, and P2, 5′-CAGGAATTCGATATCAAGCTTG-3′, were synthesized (Biotech Service Centre, University of Toronto) and separately end-labeled at their 5′ ends using [γ-^{32}P]ATP and T4 polynucleotide kinase. Three different 100-bp DNA fragments were synthesized by PCR using the plasmids pCRYSK, pPUSK, and pLBSK as templates and one 5′-end-labeled primer and the other one unlabeled as PCR primers.

PU.1 DNA Binding Domain. The PU.1 DBD consists of the amino acids 161−272 of murine PU.1. It was overexpressed and purified as described by Cheng et al. (*14*). This PU.1 construct contained an additional amino acid sequence at the N-terminus, a $(His)_6$ tag that facilitated the purification process. The $(His)_6$ tag was linked to the amino acid sequence of the PU.1 DBD with a thrombin cleavage site. This allowed us to remove the $(His)_6$ tag in the following procedure: The PU.1 DBD was dialyzed against a thrombin cutting buffer containing 50 mM Tris-HCl, pH 7.6, 150 mM NaCl, and 2.5 mM $CaCl_2$. For every 10 mg of PU.1 DBD, 20 μL of thrombin (1 unit/mL) was added in a total volume of protein solution of 10 mL. The cutting reaction was carried out overnight at 4 °C. Afterward, the PU.1 solution was dialyzed at 4 °C against a buffer containing 25 mM Na_2HPO_4, pH 6.5, and 0.1 mM PMSF. The cleavage of the $(His)_6$ tag improved the stability of the PU.1 samples and increased the possible storage duration.

Hydroxyl Radical Footprinting. The procedure used in the present experiments was modified from the original protocol (*8*). To 1 μL (20 000 cpm, ∼10 ng) of end-labeled DNA in a buffer containing 10 mM Tris HCl, pH 7.6, 50 mM NaCl, 1 mM EDTA, 1 μg of BSA, and 1 μg of poly(dI-dC)·poly(dI-dC) in a volume of 16 μL, 1 μL of PU.1 DBD at various concentrations was added, and the mixture was allowed to equilibrate at room temperature for 1 h. The footprinting reaction was carried out by adding 3 μL of cleavage solution containing 133 μM ammonium iron(II) sulfate hexahydrate solution, 266 μM EDTA, 6.7 mM sodium ascorbate, and 0.1% hydrogen peroxide. The cleavage reaction was allowed to proceed for 2 min at room temperature. It was stopped by adding 4 μL of a solution containing 50 mM thiourea and 0.1 M EDTA and then kept on ice. The reaction solutions were lyophilized and subsequently dissolved in a loading buffer containing 90% formamide.

DNase I Footprinting. End-labeled DNA (1 μL, 20 000 cpm, ∼10 ng) was incubated with 30 ng (or 300 ng) of PU.1 in 17 μL of the buffer described above, but NaCl was replaced by 10 mM $MgCl_2$ and EDTA was omitted. The complex was cleaved for 30 s at room temperature after the addition of 0.5 unit of DNase I. The reaction was stopped by adding 1 μL of a 0.2 M EDTA solution. Afterward the solution was kept on ice. The samples were dried and dissolved in loading buffer as described above.

Gel Electrophoresis. DNA samples were denatured (90 °C, 3 min) prior to loading on an 8% polyacrylamide denaturing gel (7 M urea) and run at 2000 V for 2 h. After

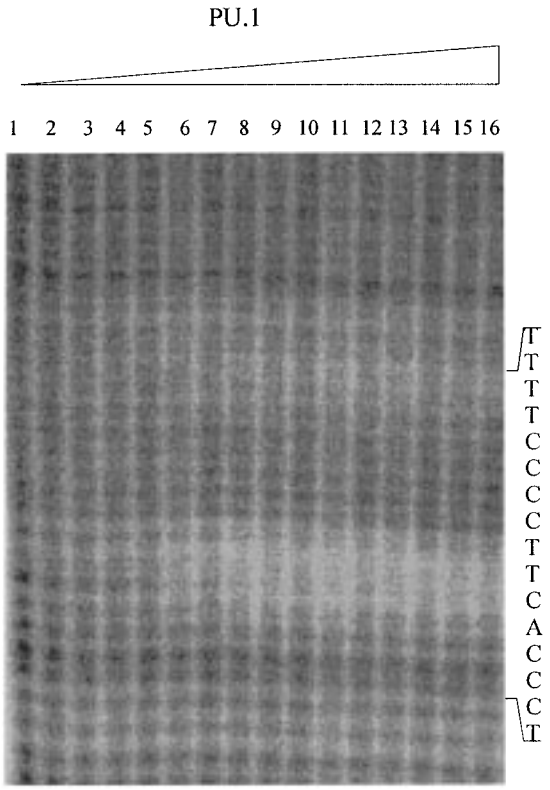

FIGURE 1: Titration of the TTCC strand with PU.1 followed with hydroxyl radical footprinting. ^{32}P-end-labeled DNA (1 μL) at 20 000 cpm (~10 ng) was used in each lane. Amount of PU.1 used: lane 1, no protein; lane 2, 0.3 ng; lane 6, 3 ng; lane 16, 1.5 μg. The location of the footprint was verified using the chemical sequencing reactions for G and G + A (data not shown).

electrophoresis the gels were dried and the band pattern was visualized using an Ambis model 4000 radioanalytic imaging system.

RESULTS

The three DNA fragments used in our experiments have been shown to bind to PU.1. pCRYSK contains the DNA sequence of the DNA−PU.1 ets domain complex in the crystal structure (*5*). pPUSK contains a 17-bp region of the SV40 enhancer known to bind PU.1 (*11*). The specific binding of the ets domain of PU.1 to this DNA region has been shown by mobility shift assays (*14*) and NMR experiments (P. E. Morin and C. H. Arrowsmith, personal communication). The third DNA target sequence used here is found on the λB site of an Igλ 2−4 enhancer (*12*). The sequence-specific binding of PU.1 to the λB site has been demonstrated by mobility shift experiments and methylation interference assays (*12*). For all three DNA fragments, we have analyzed the hydroxyl radical cleavage patterns of both strands.

Hydroxyl Radical Cleavage Pattern for the DNA Sequence Used in the Crystal Structure. The results for the DNA strand containing the antisense TTCC sequence are shown in Figure 1. Lane 1 shows that in the absence of protein a uniform cleavage pattern of the DNA is observed. Lanes 2−16 show the effect of increasing PU.1 concentration on the cleavage pattern. At a PU.1 concentration of 150 pg/μL (lane 6) a clear protection site can be detected. A second, weaker protection site is also visible. The appearance of a concentration-dependent cleavage protection is evidence of

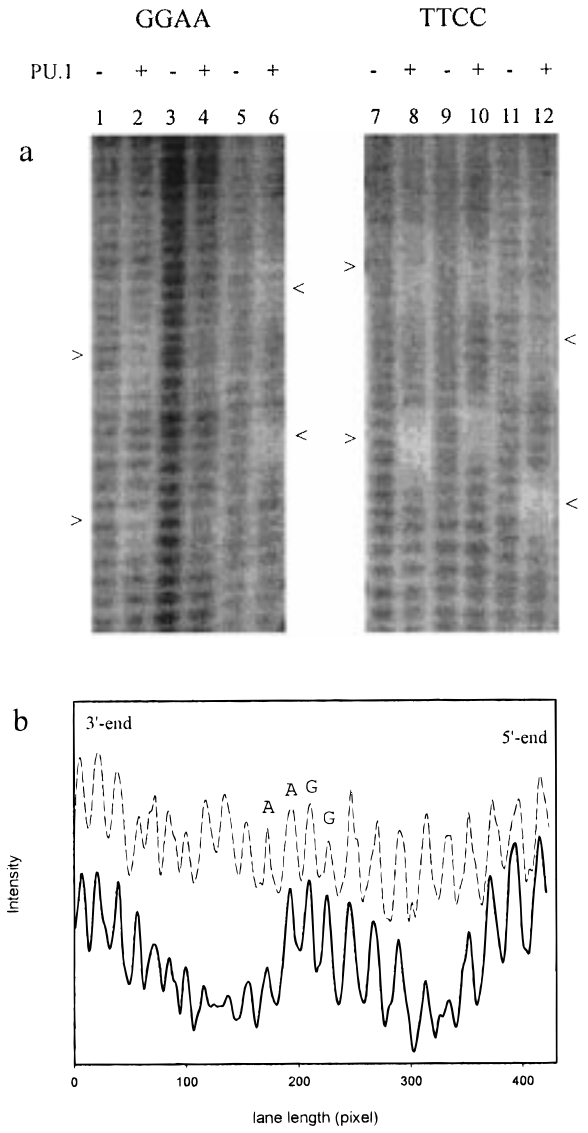

FIGURE 2: Hydroxyl radical protection pattern for the different DNA fragments used. (a) Gel region that contains the footprints observed for different DNA fragments. Each lane contains 20 000 cpm of ^{32}P-end-labeled DNA (~10 ng). The amount of PU.1 used was none (− lanes) or 300 ng (+ lanes). pCRYSK is used in lanes 1 and 2 (GGAA strand) and lanes 7 and 8 (TTCC strand), pLBSK in lanes 3 and 4 (GGAA strand) and lanes 9 and 10 (TTCC strand). The protection sites observed for these DNA fragments are marked with arrowheads on the left site of the gel. pPUSK is shown in lanes 5 and 6 (GGAA strand) and lanes 11 and 12 (TTCC strand). The protection sites obtained for this DNA fragment are indicated with arrowheads to the right. (b) The cleavage protection on the GGAA strand of the pCRYSK−PU.1 complex (lanes 1 and 2 in panel A) is demonstrated in intensity profiles. The dashed plot shows the intensity profile obtained in the absence of PU.1; the solid line represents the cutting pattern in the presence of 300 ng of protein. The overall intensities of the lanes were normalized to eliminate variation due to loading errors resulting in the intensity profiles shown here. The intensity plot of the control lane was moved along the abscissa to visualize both profiles more easily.

a specific interaction between DNA and PU.1. The protected region includes one nucleotide of the antisense TTCC core (T at position 10) and the three nucleotides upstream, C(11), A(12), and C(13); the numbering system for the DNA positions is shown in Figure 3. The weak protection site on this strand includes the nucleotides at positions 2 and 3, T(2)T(3).

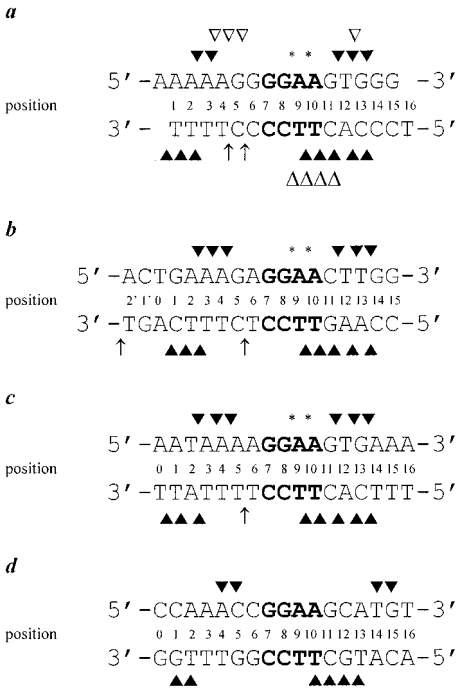

FIGURE 3: Comparison of the interactions between ets domains and their target sequences. (a) The sequence of the PU.1 binding region of the restriction fragment pCRYSK contains the DNA sequence used for crystallography of the PU.1−DNA complex (*5*). The consensus sequence is shown in boldface type; the backbone positions protected from hydroxyl radical cleavage are indicated with solid arrowheads. The base 5′ to each indicated position is missing in the gel pattern and is discussed in the text as a protected nucleotide. DNase I hypersensitive sites are marked with arrows; DNase I cleavage sites that are unchanged in the complex are marked with an asterisk. The corresponding bands in the gel pattern are the bases 5′ to an arrow or an asterisk, respectively. The contact sites described in the crystal structure are marked with open symbols (*5*). (b) DNA sequence and footprints obtained for the pPUSK−PU.1 complex. The sequence shown here is identical to that of the SV40 enhancer site (*11*). (c) Footprints obtained for the pLBSK−PU.1 complex. The sequence aligned here corresponds to the λB site of the Ig λ2−4 enhancer (*12*). The protection pattern summarized in panels a−c are obtained from several independent footprinting experiments that gave identical results. (d) Sequence positions protected from hydroxyl radical cleavage as observed in an ETS-1−DNA complex; sites showing >40% protection are indicated (*2*).

The cleavage pattern obtained for the DNA strand containing the recognition sequence is shown as raw data in Figure 2a (lanes 1 and 2) and as intensity profiles in Figure 2b. Two protection sites are found. One is upstream from the GGAA site and consists of the DNA positions A(2) and A(3). The second protection site is downstream and includes the nucleotides at the positions G(11), T(12), and G(13). Compared to the intense protection site obtained for the TTCC strand, the protected regions in the sense strand are less pronounced. Their position and the extent of protection can be determined by comparison of the normalized intensity profiles of the lanes as shown in Figure 2b. Thus, despite some apparent interactions with the protein, the nucleotides of this strand are more accessible to attack by the hydroxyl radicals than those of the TTCC strand. Interestingly, no protection occurs at the GGAA recognition site; in fact, the DNA positions G(8) and the adjacent A(9), both within the recognition sequence, are hypersensitive toward the cleavage reaction.

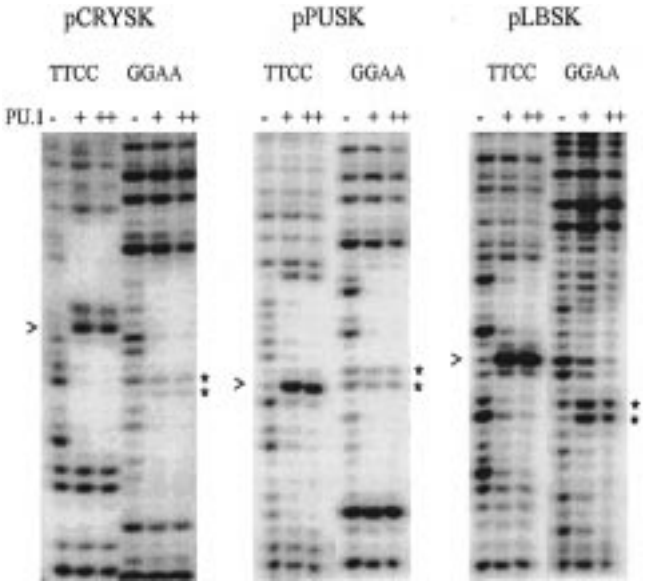

FIGURE 4: DNase I footprints of the different DNA fragments used. Each lane contains 20 000 cpm ^{32}P-end-labeled DNA (∼10 ng). Amount of PU.1 used is indicated in the following manner: no PU.1 (− lanes), 30 ng (+ lanes), and 300 ng (++ lanes). Hypersensitive sites are marked with arrowheads, and cleavage sites that are almost unchanged in the presence of PU.1 are indicated with asterisks.

Hydroxyl Radical Cleavage Pattern for the SV 40 and λB DNA Sequences. Figure 2a shows the hydroxyl radical cutting patterns obtained for the three different DNA fragments used. Lanes 1−6 give the footprints for the respective GGAA strands. With one exception, the position and the extent of the two protection sites are identical for the different sequences. The footprint downstream of the GGAA recognition sequence consists of two nucleotides in the case of pCRYSK (lane 2) and of three nucleotides for pPUSK and pLBSK (lanes 4 and 6). The interactions of PU.1 with the different DNA sequences are summarized in Figure 3.

The hydroxyl radical footprints of the PU.1 complexes on the TTCC strands of the λB site and the SV40 enhancer site are shown in lanes 9−12 in Figure 2a. To allow a direct comparison with the footprints of the pCRYSK−PU.1 complex, lanes 7 and 8 contain the footprinting data already presented in lanes 1 and 15 of Figure 1. It is evident that the cleavage patterns are identical.

The apparent shift in the protected regions of the SV40 enhancer site (as seen in lanes 6 and 12) relative to the footprints observed for pCRYSK and pLBSK arises because this sequence is inserted into pPUSK in the opposite direction. In addition, the primers used for amplification of the DNA fragments are not equally distant from the *Hin*dIII cloning site resulting in a different position of the recognition site on this DNA fragment.

DNase I Footprinting. We also compared the hydroxyl radical footprints with those obtained by DNase I cleavage for the three different DNA−PU.1 complexes. The cutting patterns observed on both strands of the DNA fragments are shown in Figure 4. The protected regions are much larger and include 16 nucleotides; the entire regions shown in Figure 3 are protected through interactions with the protein. An expansion of the apparent protection region is expected when a larger cutting reagent, such as an enzyme, is used.

An interesting feature of the DNase I footprint is the appearance of a hypersensitive band on the TTCC strand almost in the center of the protected region. The position of this band is identical for the three DNA fragments used and corresponds to nucleotide position 6. Additional DNase I hypersensitive sites are seen in the DNA fragment pCRYSK at position C(5) and another one in the DNA fragment pPUSK at position T(2′). The intensity of the latter two hypersensitive sites is less pronounced than that of position 6 but nevertheless evident. The DNase I footprints observed for the GGAA strands show that the cleavage of the DNA backbone at positions 8 and 9 remains almost unchanged in the presence of PU.1. These DNA positions are marked with asterisk.

DISCUSSION

Hydroxyl Radical Protection Pattern for the pCRYSK−PU.1 Complex. The cutting patterns observed for the pCRYSK−PU.1 complex are discussed in light of the crystallographic data for the PU.1−DNA complex (Figure 3a). The DNA sequence used in both methods is identical in the region of protein interaction. Direct contacts observed in the crystal structure between the phosphate backbone of the DNA and the protein are expected to block the access of hydroxyl radicals to those DNA positions and result in the protection of the corresponding nucleotides in the gel pattern. On the other hand, the water-mediated contacts between the protein and the DNA may allow hydroxyl radicals access to the corresponding DNA phosphate positions to at least some extent.

For the antisense strand we have observed a protected region of five bases upstream from the "anticonsensus" sequence, TTCC. The crystal structure data also suggest that there are numerous contacts between four phosphates in the DNA backbone of this strand and the protein (*5*). These contacts arise from interactions of both the main-chain and side-chain atoms of the protein with the DNA. Comparison of the binding sites obtained by the two methods reveals the protected region determined by footprinting (nucleotides 10−14) to be shifted upstream relative to that expected from the crystal structure data (nucleotides 9−12). Starting from the 5′ end, the first three DNA positions of the footprint, T(10), C(11), and A(12), are protected as expected from the contacts presented in the crystal structure. However, despite the defined contact in the crystal structure from lysine 223, the phosphate group of T(9) is not protected from hydroxyl radical cleavage. There are several possible explanations for this result. The observed cleavage of the DNA backbone reflects the accessibility of water in this region of the DNA−PU.1 complex and the crystal structure shows a network of water molecules at the recognition sequence in this region. In solution, these water molecules exchange rapidly with the bulk solvent and would allow hydroxyl radicals access to the DNA backbone. Furthermore, the bending of the DNA, shown in the crystal structure, would distort the DNA helix, widening the minor groove by 2−3 Å and making the backbone more accessible to hydroxyl radicals (*5*). On the other hand, several phosphate groups on the TTCC strand are protected from hydroxyl radical cleavage that do not have direct protein contacts in the crystal structure. These include C(13) and C(14) within the main protection site as well as T(1)T(2)T(3) at the distal end of the complex.

The hydroxyl radical cutting pattern obtained for the GGAA strand of pCRYSK also reveals differences in the protection sites compared to those expected on the basis of direct protein contacts reported in the crystal structure. In the crystal structure, one contact downstream from the core sequence was observed at the nucleotide T(12). In the footprinting experiments, this DNA position, T(12), and the two adjacent nucleotides, G(11) and G(13), are protected from cleavage. Both of these guanines are complementary to DNA positions protected on the TTCC strand. The GGAA strand shows a second site located upstream from the recognition sequence that is protected by the presence of the protein. The crystal structure reveals contacts flanking the 5′ sequence of the core at the DNA positions A(3), A(4), and G(5). In solution, only A(3) and A(2) are protected from radical cleavage. Nucleotide position A(4) is protected in the two other PU.1−DNA complexes; this is the only difference observed between the hydroxyl radical protection patterns of the different DNA sequences used here. The nucleotide position G(5) is not protected in any of the PU.1−DNA complexes analyzed despite the interactions described in the crystal structure.

From the gel pattern it is evident that, overall, the GGAA strand is more accessible to the hydroxyl radicals than the TTCC strand, resulting in a weaker footprint and the observed hypersensitivity of the DNA at positions 8 and 9 (intensity profile in Figure 2b). This observation coincides with the protein−DNA contacts observed with the GGAA strand in the crystal structure, where almost all interactions of the protein are with the bases at the recognition site, GGAA (*3*). The phosphate backbone is exposed in the wide minor groove of the bent DNA helix, which would allow attack by hydroxyl radicals even at a protein interaction site, nucleotide position G(5). In addition, the presence of numerous water molecules in the major groove around the recognition site would enhance the access of the hydroxyl radicals and lead to the hypersensitivity observed in the recognition site, since the hydroxyl radicals attack the DNA backbone via the major and the minor grooves.

It is not clear whether the differences between observed and expected protection sites are due to real differences in the solution and crystal forms of the PU.1−DNA complex or to the fact that phosphates need not be in direct contact with the protein in order to be protected from hydroxyl radical cleavage. Examination of the crystal coordinates (*5*; PDB accession code 1PUE) shows that all the protected sites here are in close proximity to the protein, specifically to the two loops N-and C-terminal to the recognition helix of PU.1. It is possible that the close proximity of the protein to the phosphate backbone in these regions could slow the cleavage reaction enough to create a footprint. Additional detailed comparisons between other crystal structures and high-resolution footprinting data are needed to understand the correspondence between these two methods.

The following factors may also contribute to the observed differences. The crystal structure was defined for amino acids 171−258 of a PU.1 fragment containing amino acids 160−272. Residues 160−170 are not resolved in the crystal structure, presumably due to the absence of an ordered conformation. The PU.1 DNA binding domain used in our experiments also contained these amino acids. The greatest difference between the footprinting data and the direct

contacts in the crystal structure occur in the vicinity of lysine 171, the first amino acid resolved in the crystal structure. Crystallographically unresolvable interactions between the DNA and the protein in this region may be responsible for the differences.

The crystals of the PU.1−DNA complex were obtained under experimental conditions that vary markedly from our experimental procedure (*15*). Within the crystal, there is end-to-end stacking of the DNA strands, as well as interactions between the protein and DNA in neighboring unit cells (*15*). In a single PU.1−DNA complex as present in our footprinting experiments, the DNA might wrap around the protein even more tightly, resulting in additional interactions that are seen on the edges of the footprint of the TTCC strand, C(13)C(14) and T(1)T(2)T(3).

Footprinting Results for the Three Different DNA Sequences. The complexes formed between PU.1 and the three DNA sequences presented here result in similar hydroxyl radical footprints. The number of protein interaction sites and their position is the same for the DNA sequence used in the crystal structure as for the two natural PU.1 target sites. The only difference observed is a missing protection of one nucleotide in the pCRYSK−PU.1 complex. The different flanking sequences in the DNA fragments we used can be compared to a Spi-1/PU.1 consensus binding site, AAAA(A/t)(G/c)(A/C/G)**GGAA**(G/c)T(A/G)(G/C), where lowercase letter indicate less-favored nucleotides (*16*). Interestingly, only the DNA sequence used in the crystal structure agrees completely with the consensus binding site, whereas both natural PU.1 binding sites differ to some extent. The close correspondence in the footprinting data for all three PU.1 binding sequences shows that PU.1 binds to various GGAA sites in a very similar manner. We hypothesize that the interaction sites of PU.1 presented here can be extrapolated to other PU.1−DNA complexes with different flanking sequences. Quantitative hydroxyl radical footprinting revealed that the ets domain of PU.1 bound the sequence used in the crystal structure (pCRYSK) and the SV40 enhancer sequence (pPUSK) with almost identical binding affinities, whereas it bound significantly more strongly the λB DNA sequence (pLBSK) (P. Gross et al., unpublished results). The identical binding mode of PU.1 to the three different DNA sequences and the high sequence homology (compare pCRYSK and pLBSK) that results in different binding affinities indicate that the affinity of PU.1 to its target sequences is at least partially also determined by additional factors that still have to be elucidated.

DNase I Footprinting. The DNase I protection pattern for the TTCC strand of PU.1−DNA complexes agrees with previous observations of a DNase I hypersensitive site near the TTCC sequence (*17*−*19*). DNase I footprints including the existence of a hypersensitive site are the same for other ets domains (ETS-1, Fli-1, and GABP), implicating a similar DNA binding mode for all ets proteins (*2, 20*). Our results are consistent with these previous findings. The analysis of three different PU.1−DNA complexes shows a highly conserved DNase I hypersensitive site one base downstream from the TTCC site. Its position relative to the recognition core was identical despite its different sequences.

The appearance of a hypersensitive site may be a consequence of the bend in the DNA introduced by protein binding. Bending the DNA fragment toward the protein molecule widens the minor groove of the DNA, presumably facilitating access by the DNase I to the backbone between C(5) and T(6) and in the pCRYSK−PU.1 complex between T(4) and C(5) as well. However, the presence of a specific hypersensitive site is difficult to rationalize on the basis of the crystal structure data, which indicate uniform bending and no apparent local distortion of the DNA helix (*5*). The second hypersensitive site in the PU.1 complex with the DNA sequence (pCRYSK) further underscores this contradiction. Elsewhere in the binding site, the presence of bound PU.1 blocks enzymatic activity of DNase I. Since hydroxyl radical footprinting did not give excess cleavage at the position of DNase I hypersensitivity, the aqueous environment around these nucleotides, C(5) and T(6), is not significantly different from the environment surrounding other unprotected DNA positions.

Our data also show the existence of a second but less hypersensitive band at the distal end of the DNase I footprint of the pPUSK−PU.1 complex. Since no other bands outside the footprint region increase in intensity in the presence of the protein, the excess cleavage at the 3′ end of the PU.1−pPUSK complex and also at position C(5) in the PU.1-pCRYSK complex is the result of a PU.1-induced change of the DNA structure and not the consequence of mass action.

The DNase I footprints observed for the GGAA strands agree with the results from hydroxyl radical footprinting. The lack of protection of the nucleotides at positions G(8) and A(9) from DNase I cleavage is consistent with the excess cleavage of the recognition region by hydroxyl radicals.

Comparison with Footprinting Data of Other Ets−DNA Complexes. The hydroxyl radical protection pattern of the PU.1−DNA complex is comparable but not identical to high-resolution footprinting data of the ETS-1−DNA complex (*2*). This is illustrated in Figure 3d. Two protection sites were found on the TTCC strand of the ETS-1−DNA complex. Their positions are identical to the protection sites found in the PU.1−DNA complexes, although the nucleotides protected from cleavage vary. The interaction sites of ETS-1 and PU.1 on the GGAA strands are comparable as well. Again, two protection sites are observed; however, their positions and the number of nucleotides involved differ in the ETS-1−DNA complex and the PU.1−DNA complexes. The comparable interaction sites of ETS-1 and PU.1 with DNA demonstrate a similar binding mode of both proteins with DNA.

Ethylation interference data of a PU.1−DNA complex suggest that a number of DNA−phosphate groups form interactions with the protein that are not observed in the hydroxyl radical footprinting experiments (*17*). The smaller size of hydroxyl radicals allows them to react with the DNA backbone at positions that are inaccessible to the somewhat larger ethyl groups. Therefore, hydroxyl radical footprinting yields a higher resolution footprint than that obtained by ethylation interference assays. Since it reflects the accessibility of water to DNA molecules, only close contacts between the protein and the DNA result in the presence of a protection site, whereas more distant interactions do not protect the DNA from radical cleavage.

The use of these two different footprinting methods, ethylation interference and hydroxyl radical footprinting, also revealed different apparent interactions in the ETS-1−DNA complex. The presence of a second protection site in

hydroxyl radical footprinting of on the TTCC strand in the ETS-1−DNA complex is not demonstrated in ethylation interference experiments of the full-length ETS-1 and its ets domain (*2*). Ethylation interference assays of other ets domains, Fli-1, GABP, and ETS-1, with different target sequences are almost identical, indicating one protein contact site on the TTCC strand (*19*). However, these data also suggest the existence of only a single protein interaction site on the GGAA strand, whereas hydroxyl radical footprinting of the ETS-1−DNA complex and as presented here for the PU.1−DNA complex showed that there is a second interaction site. From the global structure of the complexes formed by these two proteins and the information obtained from the application of different footprinting techniques to other ets proteins, it is evident that the complexes of ets proteins with DNA are comparable.

In summary, hydroxyl radical footprinting reveals detailed information about specific contacts between the DNA and the ets domain of PU.1 that are not easily accessible with other techniques. These data together with previously published work support a model for a similar mode of binding for all ets proteins with small but significant differences in the contacts flanking the GGAA site depending on sequence and experimental conditions.

ACKNOWLEDGMENT

We thank Dr. P. Morin for helpful discussions and Dr. A. Yee for preparation of PU.1 samples.

REFERENCES

1. Wasylyk, B., Hahn S. L., and Giovane, A. (1993) *Eur. J. Biochem. 211*, 7−18.
2. Nye, J. A., Peterson J. M., Gunther, C. V., Jonsen, M. D., and Graves, B. J. (1992) *Genes Dev. 6*, 975−990.
3. Donaldson, L. W., Peterson, J. M., Graves, B., J., and McIntosh, L. P. (1996) *EMBO J. 15*, 125−143.
4. Liang, H., Olejniczak, E., T., Mao, X., Nettesheim, D. G., Yu, L., Thompson, C. B., and Fesik, S., W. (1994) *Proc. Natl. Acad. Sci. U.S.A. 91*, 11655−11659.
5. Kodandapani, R., Plo, F., Ni, C. Z., Piccialli, G., Klemesz, M., McKercher, S., Maki, R. A., and Ely, K. R. (1996) *Nature 380*, 456−460.
6. Werner, M. H., Clore, G. M., Fisher, C. L., Fisher, R. J., Trinh, L., Shiloach, J., and Gronenborn, A. M. (1995) *Cell 83*, 761−771; erratum (1996) *Cell 87* (2).
7. Pio, F., Kodandapani, R., Ni, C.-Z., Shepard, W., Klemsz, M., McKercher, S. R., Maki, R. A., and Ely, K. R. (1996) *J. Biol. Chem 271*, 23329−23337.
8. Tullius, T. D., and Dombroski, B. A. (1986) *Proc. Natl. Acad. Sci. U.S.A. 83*, 5469−5473.
9. Tullius, T. D. (1988) *Nature 332*, 663−664.
10. Lee, S., and Hahn, S. (1995) *Nature 376*, 609−612.
11. Pongubala, J. M. R., Nagulapalli, S., Klemsz, M., McKercher, S. R., Maki, R. A., and Atchinson, M. L. (1992) *Mol. Cell. Biol. 12*, 368−378.
12. Eisenbeis, C. F., Singh, H., and Storb, U. (1993) *Mol. Cell. Biol. 13*, 6452−6461.
13. Maxam, A., and Gilbert, W. (1988) *Methods Enzymol. 65*, 499−560.
14. Cheng, X., Morin, P. E., Harms, A. C., Bruce, J. E., Ben-David, Y., and Smith R. D. (1996) *Anal. Biochem. 239*, 35−40.
15. Pio, F., Ni, C.-Z., Mitchell, R. S., Knight, J., McKercher, S., Klemsz, M., Lombardo, A., Maki, R. A., and Ely, K. R. (1995) *J. Biol. Chem. 270*, 24258−24263.
16. Ray-Gallet, D., Mao, C., Tavitian, A., and Moreau-Gachlin, F. (1995) *Oncogene 11*, 303−313.
17. Galson, D. L., Hensold, J. O., Bishop, T. R., Schalling, M., D'Andrea, A. D., Jones, C., Auron, P. E., and Housman, D. E. (1993) *Mol. Cell. Biol. 13*, 2929−2941.
18. Graves, B. J., Gillespie, M. E., and McIntosh, L. P., (1996) *Nature 384*, 322.
19. Rao, E., Dang, W., Tian, G., and Sen, R. (1997) *J. Biol. Chem. 272*, 6722−6732.
20. Gunther, C. V., and Graves, B. J. (1994) *Mol. Cell. Biol. 14*, 7569−7580.

BI972591K